RESEARCH PAPER

Fabrication of three-dimensional microfluidic channels in a single layer of cellulose paper

Xiao Li · Xinyu Liu

Abstract Three-dimensional microfluidic paper-based analytical devices (3D-µPADs) represent a promising platform technology that permits complex fluid manipulation, parallel sample distribution, high throughput, and multiplexed analytical tests. Conventional fabrication techniques of 3D-µPADs always involve stacking and assembling layers of patterned paper using adhesives, which are tedious and time-consuming. This paper reports a novel technique for fabricating 3D microfluidic channels in a single layer of cellulose paper, which greatly simplifies the fabrication process of 3D-µPADs. This technique, evolved from the popular wax-printing technique for paper channel patterning, is capable of controlling the penetration depth of melted wax, printed on both sides of a paper substrate, and thus forming multilayers of patterned channels in the substrate. We control two fabrication parameters, the density of printed wax (i.e., grayscale level of printing) and the heating time, to adjust the penetration depth of wax upon heating. Through double-sided printing of patterns at different grayscale levels and proper selection of the heating time, we construct up to four layers of channels in a 315.4-µm-thick sheet of paper. As a proof-of-concept demonstration, we fabricate a 3D-µPAD with three layers of channels from a paper substrate and demonstrate multiplexed enzymatic detection of three biomarkers (glucose, lactate, and uric acid). This technique is also compatible with the conventional fabrication techniques of 3D-µPADs, and can decrease the number of paper layers required for forming a 3D-µPAD and therefore make the device quality control easier. This technique holds a great potential to further popularize the use of 3D-µPADs and enhance the mass-production quality of these devices.

Keywords Paper-based microfluidics · Point-of-care diagnostics · Three-dimensional paper channels · Wax printing · Analytical tests · Multiplexed detection

1 Introduction

Microfluidic paper-based analytical devices (µPADs) represent a promising platform technology for bioanalysis featuring low cost, ease of fabrication and operation, and equipment independence (Martinez et al. 2008a; Yetisen et al. 2013). These devices are particularly suitable for use at the point of care and/or in resource-poor settings, where centralized medical facilities are not available and the cost of diagnosis is a major concern (Martinez et al. 2010). µPADs with three-dimensional (3D) channels (3D-µPADs) have also been invented through stacking multiple layers of patterned paper and connecting paper channels in different layers together (Martinez et al. 2008b). Compared to the two-dimensional (2D) configuration (in which paper channels are patterned on a single-paper substrate), 3D paper channels allow fluid flows to run both laterally and vertically and thus enable 3D, complex fluid manipulations and more flexible device designs. With the same footprint, 3D-µPADs could incorporate more channels, fluid control components, and more reaction zones than single-layer µPADs.

X. Li · X. Liu (✉)
Department of Mechanical Engineering, McGill University,
817 Sherbrooke Street West, MD270, Montreal,
QC H3A 0C3, Canada
e-mail: xinyu.liu@mcgill.ca

Despite these advantages of 3D-µPADs, the majority of existing µPAD designs used 2D rather than 3D channels (Martinez et al. 2007; Li et al. 2008; Nie et al. 2010; Lutz et al. 2011; Ge et al. 2012b; Zuo et al. 2013), largely due to the tedious fabrication process of 3D-µPADs. The original fabrication technique (Martinez et al. 2008b), developed by the Whitesides Group, involves aligning and then stacking layers of patterned paper and double-sided adhesive tape to form 3D channels. Cellulose powder or shaped paper pieces is used to fill holes in the tape layers and bridge channels in adjacent paper layers (Martinez et al. 2008b; Noh and Phillips 2010). The potential issues during device fabrication using this technique include misalignment of paper/tape layers and discontinuity of channels in adjacent paper layers (due to improper filling of holes in the tape layers). The alignment of paper/tape layers could be avoided through folding of patterned paper into multilayer devices (Liu et al. 2012; Ge et al. 2012a). However, this folding-based approach still requires a clamping holder for mechanically maintaining the stacked device. Therefore, the current fabrication techniques of 3D-µPADs raise challenges in device manufacturing and quality control, which is especially true in mass production.

Recently, two solutions for simplifying the fabrication of 3D-µPADs have been proposed. The Phillips Group introduced a parallel fabrication process in which large pieces of paper, each of which includes an array of duplicated channels, were aligned and bonded together using spray adhesive, and then cut into individual multilayer devices (Lewis et al. 2012). It provides a higher throughput of fabrication by simultaneously aligning and stacking multiple devices in parallel. In the reports from the Martinez Group, toner was laser-printed as both impermeable barrier and adhesive to confine fluids in single-layer channels and bond layers of patterned paper to form a 3D-µPAD (Schilling et al. 2012, 2013).

In this work, we propose a wax-printing-based technique for fabricating 3D channels in a single layer of cellulose paper. Interconnected layers of paper channels are patterned at different levels along the thickness of a paper substrate, by controlling the penetration depth of the melted wax from both sides of the paper and thus forming 3D hydrophobic barriers. We demonstrate that up to four layers of channels can be fabricated in Whatman® 3MM chromatography paper (315.4 µm thick) without process optimization. The 3D architecture of the channel network in a paper substrate can be readily controlled by adjusting two parameters: (1) density of printed wax (through controlling the grayscale level of wax printing), and (2) heating time (for melting the wax). This technique is also compatible with these conventional fabrication techniques of 3D-µPADs and can decrease the number of paper layers required for constructing 3D-µPADs.

2 Experimental design

Since solid wax printing was applied to patterning microfluidic channels on cellulose paper (Carrilho et al. 2009; Lu et al. 2009), this technique has been widely used because of its high simplicity and efficiency. The principle of wax-printing-based paper patterning is based on the capillary wicking of melted wax (which is initially printed on one side of the paper) through the whole thickness of porous paper upon heating, forming hydrophobic wax barriers and 2D hydrophilic paper channels. In this work, we extended the capability of solid wax printing to patterning of 3D paper channels in a single sheet of paper, through controlling the penetration depth of the melted wax. Instead of printing the wax on one side of the paper substrate and allowing the melted wax to wick through the complete thickness of the paper during heating, we printed wax on both sides of the paper and controlled the penetration depth of the melted wax from both sides to fabricate 3D hydrophobic barriers along the paper thickness and thus form 3D hydrophilic paper channels.

We adjusted two fabrication parameters to control the penetration depth of wax printed on paper surfaces during heating. (1) *Density of printed wax:* We changed the grayscale level of wax printing to deposit wax to the paper surfaces with different densities. Once heated, we observed that high-density wax wicked faster along the paper thickness than low-density wax, resulting in hydrophobic barriers with different thickness values formed in the paper. In the eight-bit RGB color system we used in AutoCAD®, a grayscale color is displayed when the RGB values are equal. This RGB (red–green–blue) color system is converted to the CMYK (C: cyan; M: magenta, Y: yellow, and K: key or black) color system of the wax printer during printing. Figure 1a shows microscopic photographs of CMYK-colored solid wax microdots printed on top of chromatography paper with different grayscale values. The grayscale intensity changed from pure black (grayscale value = 0) to pure white (grayscale value = 255; no wax deposited). At a lower grayscale value (darker), the wax microdots in CMYK colors were printed at a higher density (Fig. 1a). While being heated, high-density wax microdots had less lateral space to wick and thus travelled faster vertically (along the paper thickness) than low-density ones. (2) *Heating time:* With the same density of wax printed on paper, longer heating time led to deeper penetration into the paper. One can also adjust the heating temperature to control the penetration depth of the melted wax. After the glass transition point, higher temperature makes the melted wax less viscous and thus wick faster (Ohta and Rosen 2006). We opted not to examine the heating temperature for simplifying the experimental design.

Fig. 1 Formation of 3D microfluidic channels inside a single sheet of Whatman® 3MM chromatography paper (315.4 μm thick). **a** Microscopic photographs of wax microdots printed at different RGB (or *grayscale*) levels. The printing intensity changes from *pure black* [*grayscale* 0 or RGB (0, 0, 0)] to *pure white* [*grayscale* 255 or RGB (255, 255, 255)]. **b**, **c** Schematic illustrations of the formation of **b** two-layer and **c** four-layer channels. In (**b**), both sides of the paper were printed at the same *grayscale* level (color figure online)
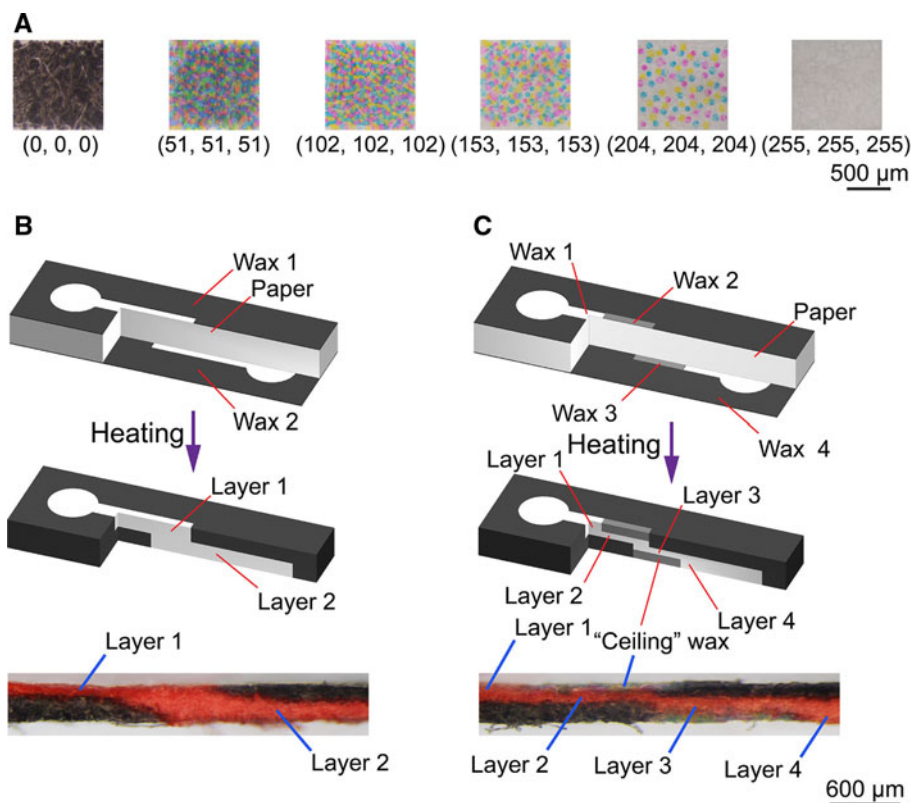
We chose Whatman® 3MM chromatography paper as the substrate material. Its thickness was measured to be 315.4 ± 6.9 μm ($n = 5$), greater than that of Whatman No. 1 chromatography paper (~ 180 μm) commonly used in μPAD fabrication; it provides more space along paper thickness for fabricating 3D channels. Figure 1b, c schematically illustrates the formation of 3D channels in one-time printing and heating. In the first kind of designs (Fig. 1b), channel layers were formed through alignment of un-patterned paper areas on both sides of the paper substrate. Both sides of the paper were printed at the same grayscale level (the same density). Once heated, the wax from both sides wicked into the paper and formed hydrophobic walls of two interconnected layers of channels. The heating time was controlled to adjust the penetration depth of the melted wax. The overlap of the un-patterned paper areas formed a vertical interconnect between the two channel layers. In another kind of designs (Fig. 1c), different areas on each side of the paper were printed with wax at different grayscale (wax density) values. As high-density wax wicked faster than low-density wax upon heating, two layers of open channels (layers 1 and 4) and two layers of enclosed channels (layers 2 and 3) can be formed. Although we demonstrated fabrication of up to four layers of channels in Whatman® 3MM paper, one can achieve, in principle, more than four layers of channels using this technique.

3 Materials and methods

3.1 Materials

All the chemicals employed in this study were purchased from Sigma-Aldrich Canada and used as received without further purification. Biomarker analytes in the colorimetric tests were D-(+)-glucose (99.5 %), sodium L-lactate (98 %), and uric acid (99 %). Accordingly, glucose oxidase (from *Aspergillus niger*, 147,900 units/g), lactate oxidase (from *Pediococcus* sp., 35 units/mg), and uricase (from *Candida* sp., 4.9 units/mg) were, respectively, mixed with peroxidase type I (from horseradish, 50 units/mg) as oxidizers. Trehalose was mixed with the enzymes for stabilization. A mixture of 4-aminoantipyrine and 3,5-dichloro-2-hydroxy-benzenesulfonic acid was used as the oxidation indicator. Details of chemical concentrations and mixing ratios are listed in Table S1. We prepared artificial urine solution following a previously reported protocol (Brooks and Keevil 1997; Zhao et al. 2013). The artificial urine solution contained 170 mM urea, 1.1 mM lactic acid, 2 mM citric acid, 25 mM sodium bicarbonate, 2.5 mM calcium chloride, 90 mM sodium chloride, 2 mM magnesium sulfate, 10 mM sodium sulfate, 7 mM potassium dihydrogen phosphate, 7 mM dipotassium hydrogen phosphate, and 25 mM ammonium chloride, all mixed in deionized (DI) water. The pH of the solution was adjusted

to 6 by adding 1 M hydrochloric acid. Paper device was fabricated from Whatman® 3MM chromatography paper (Sigma-Aldrich, Canada).

3.2 Calibration of wax penetration depth

To provide design guidelines of this technique, we calibrated the penetration depth of melted wax as a function of the grayscale value and the heating time. We used 100 °C as the heating temperature in all experiments. We first drew 5×5 mm^2 squares in AutoCAD® 2013 student version (AutoDesk, CA, USA), filled them with solids at grayscale values of 0, 51, 102, 153, 204, and printed them out on 3MM chromatography paper using a Xerox ColorCube 8570 printer. We then heated the wax-printed paper pieces in an oven at 100 °C for certain periods of time to allow the melted wax to wick into the paper. After cooling down the paper at room temperature, we cut each patterned paper piece in half and imaged its cross sections under a stereomicroscope to

measure the penetration depth. To enhance the contrast, we stained the un-patterned paper using red food dye before imaging. The penetration depth was measured in the microscopic photographs using Photoshop® CS6 (Adobe, CA, USA).

3.3 Inspection of wax-barrier quality

Comparing to conventional μPADs, hydrophobic barriers in the 3D-μPADs we fabricated were formed in thicker chromatography paper substrates (315.4 μm) with wax printed at lower density levels. The hydrophobic barriers formed in this way could potentially have lower quality, in terms of their capability of holding aqueous solutions in paper channels, than wax barriers formed at higher printing density values on thinner paper substrates. We characterized the quality of wax barriers, formed by single-side and double-side printing, through examining the smallest size of functional wax barriers (which could hold aqueous solutions without leakage).
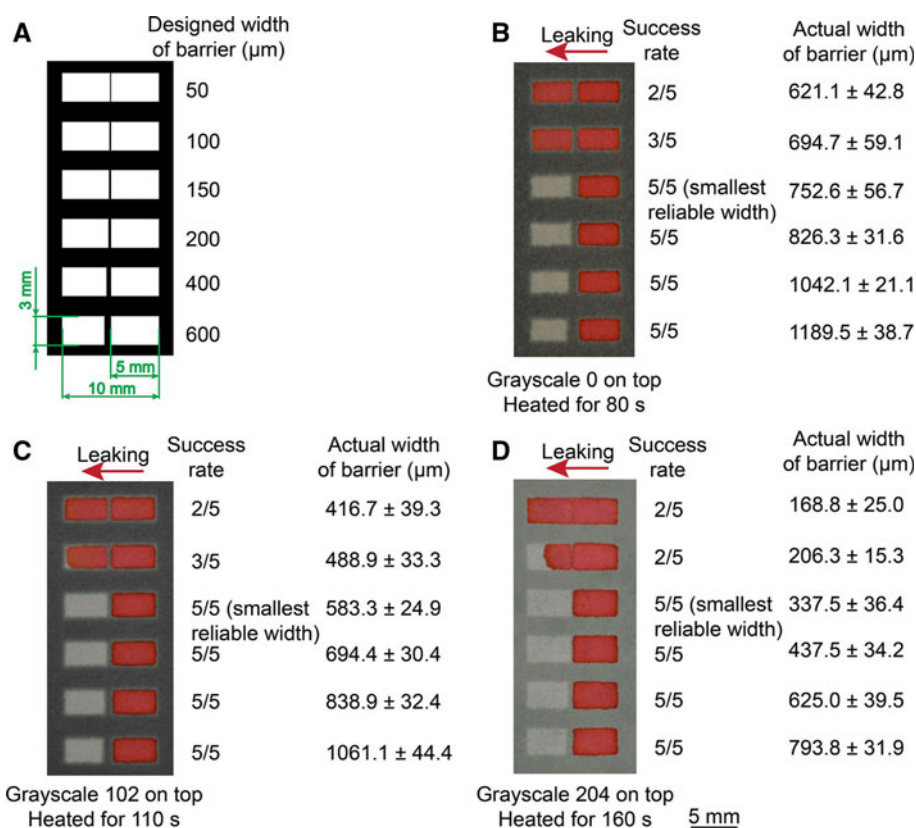
Fig. 2 Testing of wax-barrier quality using double-sided printing. Wax patterns shown in (**a**) was printed on one surface of the paper at *grayscale* 0, 102, and 204, and blanket wax was printed on the other surface of the paper at *grayscale* 0. The printed paper pieces were then heated for 80, 110, and 160 s to form complete hydrophobic barriers. *Red food dye* was added to the right paper zone to inspect potential leaks through the wax barriers. **b–d** show photographs of

devices (respectively printed at grayscale levels of 0, 102, and 204) taken 20 min after the dye was added and the results of leakage inspection. The success rate of *x/y*, at a specific combination of barrier width and *grayscale* level, means *x* out of *y* barriers successfully held the dye for 20 min without leakage. The actual width of barrier is reported in mean ± 1 standard deviation (SD) (color figure online)

In our 3D fabrication technique, wax patterns printed at different grayscale levels are used to form the barriers (Fig. 1b, c). Dark wax patterns shall form more hydrophobic barriers than light ones as it has more wax per unit area to wick through the pores of paper. On the other hand, light wax patterns wick shorter distances laterally and thus form narrower wax barriers given the same period of heating time. To probe the limit of dimension at which functional wax barriers could be formed, we used three grayscale values (0, 102, and 204), to print wax patterns on one side or both sides of Whatman® 3MM chromatography paper and form hydrophobic barriers with different widths, and investigated their capability of holding red dye solution in paper channels. For single-sided printing, we printed wax patterns at grayscale = 0 on one side of the paper to form two un-printed rectangles side by side with a wax line in between, as shown in Fig. 2a. We varied the nominal width (set value in CAD files) of the middle wax line from 50 to 600 μm. We heated the printed paper pieces in an oven at 100 °C until the wax penetrated the whole thickness of 3MM chromatography paper and formed complete hydrophobic barriers surrounding the paper zones. For double-sided printing, we printed the same wax patterns (Fig. 2a) on one side of the paper, and blanket wax on the other side of paper, and heated the printed paper (with the side with wax patterns facing up) at 100 °C to form complete hydrophobic barriers. For heating the single-side- and double-side-printed paper, we selected the shortest heating time required for generating complete hydrophobic barriers, based on the calibration results of wax penetration depth as a function of wax density and heating time (Sect. 4.1 and Fig. 3). This led to the smallest widths of the wax barriers between two paper channels, at different grayscale levels of wax printing. We added 3 μL of red food dye to the right paper zone, and waited for 20 min before examining if the wax barrier between the two paper zones could hold the dye without leakage. We observed five samples for each printing condition.

3.4 Characterization of enclosed channels

The presented technique can form enclosed channels using 'ceiling' wax (Fig. 1c), and the height of the enclosed channels can be controlled by adjusting the penetration depth of the 'ceiling' wax. The enclosement of paper channels could potentially: (1) reduce evaporation of solutions in the channels and (2) prevent contaminations by avoiding contact between the solutions and the environment/user. We examined these two characteristics of the enclosed channels through the following experiments.

(1) *Quantification of the evaporation rate of aqueous solutions in enclosed channels:* We fabricated 64 mm × 64 mm paper reservoirs on Whatman® 3MM chromatography paper and then enclosed the reservoirs using two layers of 'ceiling' wax barriers (Fig. S1(A)). The 'ceiling' wax layers were formed through double-sided printing of wax at grayscale = 153 or 204 and subsequent heating at 100 °C for 80 s, and the thickness of the 'ceiling' wax layer was 94.9 and 75.2 μm, respectively. We added 500 μL 1 × PBS to the paper channel and measured the weight loss of PBS-added paper device every 5 min to quantifying the evaporation rate. We also measured the evaporation rate of 1 × PBS in open paper reservoirs with the same size for comparison (Fig. S1(B)). (2) *Evaluation of liquid permeability of the 'ceiling' wax barrier:* We firmly sandwiched a 45 mm × 60 mm enclosed paper channel (with two layers of 75.2-μm-thick 'ceiling' wax barriers formed through wax printing at a grayscale level of 204) using two pieces of blotting paper (Whatman GB004), passed 10 × diluted blue food dye (Food Color Preparation, Club House) through the paper channel for 15 min, and then checked if there was any leaked blue dye on the blotting paper pieces.

We quantified the wicking speed of aqueous solutions in enclosed channels with different heights. We fabricated 2-mm-wide enclosed paper channels through double-sided wax printing at different grayscale levels to adjust the channel heights (Fig. S2), passed 10 × diluted red food dye, and recorded the time for the dye to wick for a certain distance.

4 Results and discussions

4.1 Calibration data of wax penetration depth versus grayscale level and heating time

Figure 3 shows calibration results of the wax penetration depth as a function of the grayscale level and the heating time. The data revealed reproducible trends that the melted wax penetrated deeper into the paper with a lower grayscale level (i.e., higher density of printed wax) and longer heating time. We found that, with a heating period of 320 s or longer, wax printed at the grayscale level of 51 and below completely penetrated the 315.4-μm-thick 3MM chromatography paper, and that wax printed at the grayscale level of 102 also completely penetrated when heated for 480 s. Based on these calibration plots, one can find a proper combination of the grayscale level and the heating time to form wax barriers with desired penetration depth. For example, if wax with a grayscale level of 0 is printed on both sides of a 3MM chromatography paper, similar to wax 1 and wax 2 in Fig. 1b, it will take approximately 80 s for the wax to form a complete barrier across the paper thickness. Similarly, for the channel design in Fig. 1c, one can pre-calculate the height of enclosed channels to be formed when a combination of grayscale levels for wax printing on both sides of the paper is chosen.
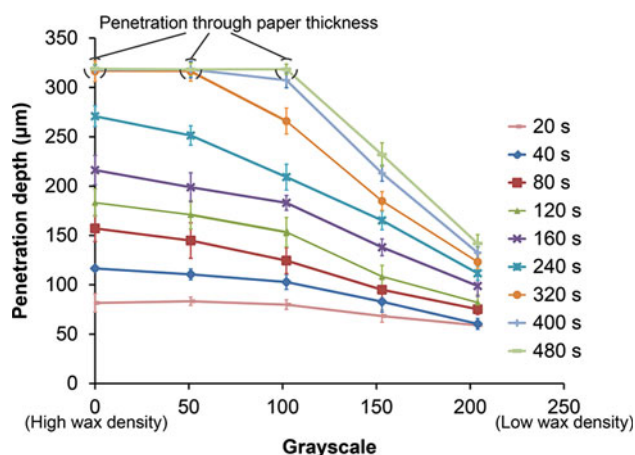
Fig. 3 Experimental results of wax penetration depth versus *grayscale* level and heating time ($N = 4$). *Error bars* represent 1 SD (color figure online)

4.2 Wax-barrier quality

For channel patterns shown in Fig. 2a, we found that wax barriers formed through single-sided printing at grayscale = 0 (corresponding to the highest wax density) had poor quality and cannot hold liquids without leakage (Fig. S3), despite the fact that the melted wax had penetrated the whole paper after heating. The leaks mainly happened on the back side of the device (opposite to the printed side) because the wax on the back side (wicked from the printing side) was insufficient to form hydrophobic barriers. The channel shapes were also severely distorted due to accumulated non-uniformity of lateral wicking of the wax during longtime heating (Fig. S3). Since we used the highest wax density in the single-sided printing, the poor barrier quality indicates that, on Whatman® 3MM chromatography paper (315.4 µm thick), wax barriers made through single-sided printing cannot function properly.

For wax barriers formed via double-sided printing, Fig. 2b–d shows typical photographs of un-leaked and leaked wax barriers with different widths and the corresponding success rates of holding the red dye without leakage (e.g., 5/5 means 5 out of 5 barriers successfully held the dye without leakage). Calculated from the calibration results of wax penetration depth (Fig. 3), the depths of barriers, formed through wax printing at grayscale levels of 0, 102, and 204 on the paper top surface, are 157.1, 146.2, and 98.8 µm, respectively. One can see that, the smallest widths of wax barriers, which can reliably hold the dye with a success rate of 100 %, are 752.6 ± 56.7 µm (grayscale = 0), 583.3 ± 24.9 µm (grayscale = 102), and 337.5 ± 36.4 µm (grayscale = 204), all with a nominal printing dimension of 150 µm. Because lower wax density leads to limited lateral wicking on paper, grayscale 204

generates a much smaller reliable barrier width (337.5 µm) than grayscale 0 (752.6 µm) and grayscale 102 (583.3 µm).

4.3 Characterization of enclosed channels

Figure S1 (C) illustrates the experimental results of the evaporated volumes of 1 × PBS versus time in 64 mm × 64 mm paper reservoirs with and without 'ceiling' wax barriers. We found that there was no difference in the evaporation rates in enclosed and open paper reservoirs, and thus concluded that the enclosement of paper channel, formed by the presented technique, cannot reduce evaporation of solutions in the channel. We attributed this finding to the fact that the melted wax only wicks through paper microfibers to form hydrophobic barriers but does not completely fill the pores of the paper to generate gas-impermeable 'ceilings' of the enclosed channels.

We tested fluid permeability of 'ceiling' wax barriers through passing blue dye through an enclosed channel sandwiched with blotting paper and inspecting any leaks from the enclosed channel to the blotting paper. For 75.2-µm-thick 'ceiling' wax barriers fabricated from printing at a grayscale level of 204, we did not observe any leak in five tests. This result confirmed that the enclosed channel can effectively prevent the solutions from contact with the environment and the user, and thus avoid potential contaminations.

Printing the 'ceiling' wax at different grayscale levels and/or heating it for different periods of time lead to different wax penetration depths and thus different height (or thickness) of the enclosed channels. We characterized the wicking speed of 1 × PBS in 2-mm-wide paper channels
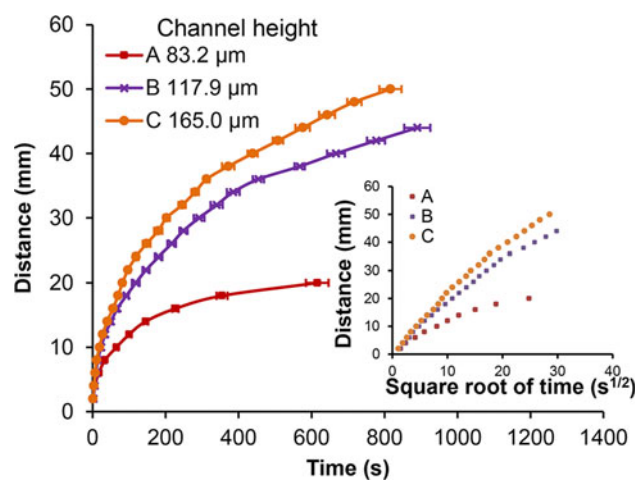

Fig. 4 Experimental results of wicking time versus distance inside 2-mm-wide enclosed channels with different channel heights ($N = 6$). The channel heights were calculated based on the data obtained through wax penetration depth calibrations. *Error bars* represent 1 SD

with heights of 83.2, 117.9, and 165.0 µm. From the measurement results shown in Fig. 4, one can find that, with the same width, higher channels transported liquid faster than shallower ones. While being plotted in the format of wicking distance versus square root of time (inset in Fig. 4), the measurement data followed straight lines in the time range of 0–12 min, and agreed with the prediction of Washburn equation (Washburn 1921). The data deviated from straight lines in longer wicking periods (>12 min) due to the effect of evaporation. Although we only performed testing of wicking speeds in enclosed channels with a typical width of 2 mm, one can readily acquire measurement data for channels with different widths by following the same experimental procedure. These characterization data can be used for designing enclosed channels with desired wicking speeds; this could be used for fluidic timing, which has been demonstrated in previous µPAD designs (Noh and Phillips 2010; Lutz et al. 2011; Li et al. 2013).

4.4 Demonstration of a 3D-µPAD for multiplexed colorimetric detection

Using the presented technique, we demonstrated the fabrication of a 3D-µPAD with three-layer channels for multiplexed colorimetric detection of glucose, lactate, and uric acid in artificial urine. The device, as illustrated in Fig. 5a, b, has a single inlet on its top side, nine test zones (three for each analyte) on its bottom side, and enclosed paper channels connecting the inlet and the test zones. Comparing to single-layer multiplexing µPADs with open or lamination-enclosed channels, our design produced enclosed branching channels through simple fabrication and does not need device packaging to prevent contaminations. The 3D-µPAD was fabricated from a single layer of 3MM chromatography paper, through double-sided printing of wax patterns at different grayscale levels (Fig. 5a). After heating the printed paper piece to form the wax barriers, labels were printed on the bottom side of the device (Fig. 5b) to indicate test zones for detecting different analytes (G: glucose, L: lactate, and U: uric acid). Colorimetric reactions for detecting the three analytes were all based on the oxidation of these analytes by corresponding oxidase enzymes, during which hydrogen peroxide was produced and the subsequent color change of colorimetric indicator was induced upon oxidation by the generated hydrogen peroxide. The details of required reagents, device preparation, and experimental conditions are described in the Online Resource.

In the experiments, we added 10 µL of artificial urine, spiked with the three analytes at different concentrations, to the device inlet, waited for 10 s to let the urine wick to the reaction zones, and measured the colorimetric signals after 10-min reactions using a desktop scanner (LiDE 210, Cannon, Japan). The analyte labels (G, L, and U) printed on the back
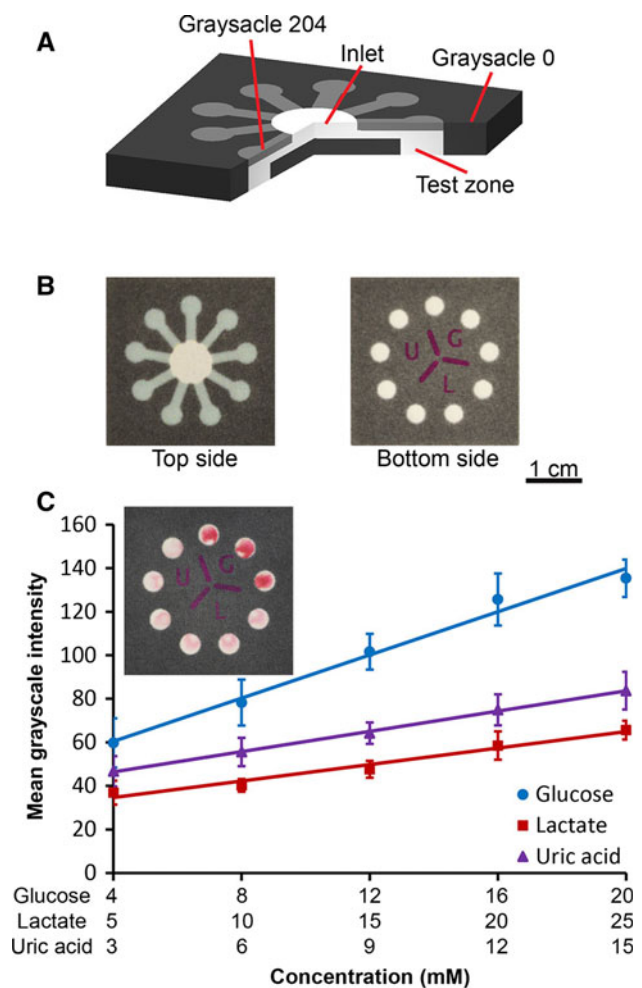

Fig. 5 A three-layer µPAD for multiplexed colorimetric detection. **a** Cross-sectional schematic of the three-layer channel structure of the µPAD. **b** Photographs of top and bottom surfaces of the µPAD. *Letters* wax printed on the *bottom sides* indicate a group of three test zones for the same marker (*G* glucose, *L* lactate, *U* uric acid). **c** Experimental results of the colorimetric intensity data versus the marker concentration (*N* = 5). *Error bars* represent 1 SD. The *inset* shows a photograph of the test zones after colorimetric reaction

side of the device made the signal measurements more straightforward, enhancing the user-friendliness of the device. The acquired data of colorimetric grayscale intensity versus concentration are plotted in Fig. 5c, and the inset shows a scanned photograph of nine test zones with colored precipitates. The glucose reactions usually generated much deeper red participate than these of lactate and uric acid. As expected, the calibration curves revealed a linear relationship of the grayscale intensity and the analyte concentrations.

4.5 Demonstration of compatibility with conventional fabrication technique of 3D-µPADs

Although the presented technique allows one to achieve multilayer of channels in one piece of paper, it cannot

Fig. 6 Photographs of multilayer devices and the illustrations of the consisting layers. **a** *Top and bottom sides* of the spot distribution device and the consisting layers. 20 μL *blue*, 80 μL *red*, and 40 μL *green* dye solutions were dropped to corresponding inlets. **b** *Top and bottom sides* of the 'McGill' logo device and the consisting layers. 60 μL *blue*, 30 μL *red*, and 30 μL *green* dye solutions were dropped to corresponding inlets (color figure online)
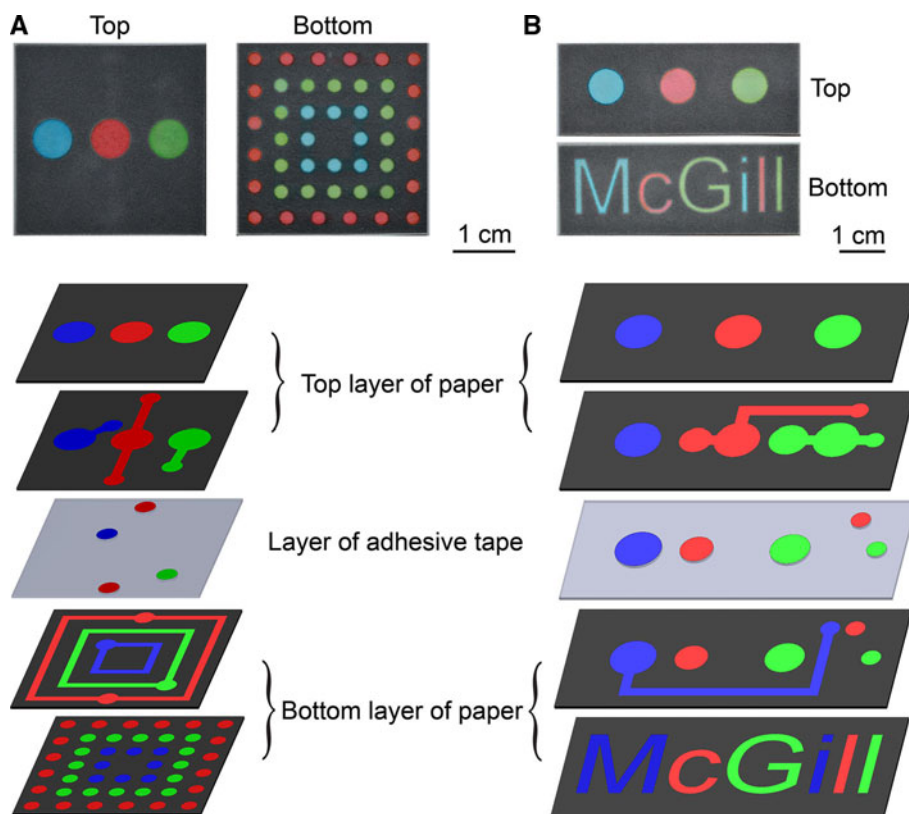
completely replace the conventional stacking-based technique for constructing 3D-μPADs. The major reason is that the presented technique cannot generate crossing channels stacked with one on top of another in the same piece of paper, given the fact that the melted wax can only penetrate into the paper from one side and thus cannot form thin-film hydrophobic wax barriers inside the paper to separate two stacked crossing channels. Another reason is that given the limited thickness of a paper substrate, the maximum number of channel layers that can be fabricated in one sheet of paper is limited (e.g., four layers of channels for a 315.4 μm 3MM chromatography paper).

However, this fabrication technique is compatible with the conventional techniques for constructing 3D-μPADs. To form a 3D-μPAD with crossing channels or with a large number of channel layers, one can use our technique to readily pattern multiple layers of 3D channels in single layers of paper, and then follow the conventional approach to stack these paper sheets together and form more complex channel networks. Here, we demonstrated the fabrication of 3D-μPADs with four-layer paper channels by stacking two layers of patterned paper, each of which contained two layers of channels fabricated using the presented technique. For fabrication of each paper layer, we printed wax on both sides of the paper at a grayscale

level = 0, and then heated the paper at 100 °C for 80 s. We used a layer of double-sided adhesive tape, laser-cut with through-holes, for adhering the two layers of patterned paper together. We employed a mixture of cellulose powder and water (w/w ratio: 1:3) to fill the through-holes of the tape layer. We made two demonstration devices, as shown in Fig. 6, to distribute dye solutions with three different colors from single inlets on the top of the devices to multiple outlets on the bottom of the devices (which could serve as test zones in analytical tests), and formed specific color patterns (an array of circular zones in Fig. 6a, and a 'McGill' logo in Fig. 6b). Both types of devices worked properly and distributed the three dye solutions into desired outlets.

In a conventional fabrication process, both devices in Fig. 6 would require four layers of paper and three layers of adhesive tapes, while only two layers of paper and one layer of tape were used in our demonstration. More importantly, the alignment/stacking steps of layers of paper and tape, which are the most tedious and challenging in the whole fabrication process, were reduced from three times to one time. Hence, we believe the presented fabrication technique, combined with the conventional stacking method, can improve the efficiency and convenience of fabricating 3D-μPADs with complex channel networks.

5 Conclusion

We reported a novel wax-printing-based technique for fabricating 3D microfluidic channels inside a single layer of cellulose paper. By controlling penetration depth of melted wax on both sides of the paper substrate, multiple layers of paper channels were formed at different levels along the paper thickness. Major fabrication parameters for controlling the penetration depth were characterized, providing guidelines for designing this type of paper-based devices. It was demonstrated that the technique allowed easy fabrication of up to four layers of paper channels in a 315-μm-thick paper substrate, without any process optimization. Using this simple technique, we created a μPAD with a three-layer channel network and demonstrated multiplexed colorimetric detection of three biomarkers (glucose, lactate, and uric acid). We also showed that the presented technique is compatible with the conventional fabrication techniques of 3D-μPADs. This technique, we believe, can significantly simply the fabrication of 3D-μPADs and improve the device quality.

References

Brooks T, Keevil CW (1997) A simple artificial urine for the growth of urinary pathogens. Lett Appl Microbiol 24(3):203–206. doi:10.1046/j.1472-765X.1997.00378.x

Carrilho E, Martinez AW, Whitesides GM (2009) Understanding wax printing: a simple micropatterning process for paper-based microfluidics. Anal Chem 81(16):7091–7095. doi:10.1021/Ac901071p

Ge L, Yan J, Song X, Yan M, Ge S, Yu J (2012a) Three-dimensional paper-based electrochemiluminescence immunodevice for multiplexed measurement of biomarkers and point-of-care testing. Biomaterials 33(4):1024–1031. doi:10.1016/j.biomaterials.2011.10.065

Ge S, Ge L, Yan M, Song X, Yu J, Huang J (2012b) A disposable paper-based electrochemical sensor with an addressable electrode array for cancer screening. Chem Commun 48(75):9397–9399. doi:10.1039/c2cc34887j

Lewis GG, DiTucci MJ, Baker MS, Phillips ST (2012) High throughput method for prototyping three-dimensional, paper-based microfluidic devices. Lab Chip 12(15):2630–2633. doi:10.1039/C2lc40331e

Li X, Tian J, Nguyen T, Shen W (2008) Paper-based microfluidic devices by plasma treatment. Anal Chem 80(23):9131–9134. doi:10.1021/ac801729t

Li X, Zwanenburg P, Liu XY (2013) Magnetic timing valves for fluid control in paper-based microfluidics. Lab Chip 13(13):2609–2614. doi:10.1039/C3LC00006K

Liu H, Xiang Y, Lu Y, Crooks RM (2012) Aptamer-based origami paper analytical device for electrochemical detection of adenosine. Angew Chem 51(28):6925–6928. doi:10.1002/anie.201202929

Lu Y, Shi WW, Jiang L, Qin JH, Lin BC (2009) Rapid prototyping of paper-based microfluidics with wax for low-cost, portable bioassay. Electrophoresis 30(9):1497–1500. doi:10.1002/elps.200800563

Lutz BR, Trinh P, Ball C, Fu E, Yager P (2011) Two-dimensional paper networks: programmable fluidic disconnects for multi-step processes in shaped paper. Lab Chip 11(24):4274–4278. doi:10.1039/c1lc20758j

Martinez AW, Phillips ST, Butte MJ, Whitesides GM (2007) Patterned paper as a platform for inexpensive, low-volume, portable bioassays. Angew Chem Int Ed 46(8):1318–1320. doi:10.1002/anie.200603817

Martinez AW, Phillips ST, Carrilho E, Thomas SW, Sindi H, Whitesides GM (2008a) Simple telemedicine for developing regions: camera phones and paper-based microfluidic devices for real-time, off-site diagnosis. Anal Chem 80(10):3699–3707. doi:10.1021/ac800112r

Martinez AW, Phillips ST, Whitesides GM (2008b) Three-dimensional microfluidic devices fabricated in layered paper and tape. Proc Natl Acad Sci USA 105(50):19606–19611. doi:10.1073/pnas.0810903105

Martinez AW, Phillips ST, Whitesides GM, Carrilho E (2010) Diagnostics for the developing world: microfluidic paper-based analytical devices. Anal Chem 82(1):3–10. doi:10.1021/ac9013989

Nie ZH, Deiss F, Liu XY, Akbulut O, Whitesides GM (2010) Integration of paper-based microfluidic devices with commercial electrochemical readers. Lab Chip 10(22):3163–3169. doi:10.1039/C0lc00237b

Noh H, Phillips ST (2010) Fluidic timers for time-dependent, point-of-care assays on paper. Anal Chem 82(19):8071–8078. doi:10.1021/Ac1005537

Ohta N, Rosen M (2006) Color desktop printer technology: optical science and engineering, vol 106. CRC Press/Taylor and Francis Group, Boca Raton, FL

Schilling KM, Lepore AL, Kurian JA, Martinez AW (2012) Fully enclosed microfluidic paper-based analytical devices. Anal Chem 84(3):1579–1585. doi:10.1021/ac202837s

Schilling KM, Jauregui D, Martinez AW (2013) Paper and toner three-dimensional fluidic devices: programming fluid flow to improve point-of-care diagnostics. Lab Chip 13(4):628–631. doi:10.1039/C2LC40984D

Washburn EW (1921) The dynamics of capillary flow. Phys Rev 17(3):273–283. doi:10.1103/PhysRev.17.273

Yetisen AK, Akram MS, Lowe CR (2013) Paper-based microfluidic point-of-care diagnostic devices. Lab Chip 13(12):2210–2251. doi:10.1039/c3lc50169h

Zhao C, Thuo MM, Liu XY (2013) A microfluidic paper-based electrochemical biosensor array for multiplexed detection of metabolic biomarkers. Sci Technol Adv Mater 14(5). doi:10.1088/1468-6996/14/5/054402

Zuo P, Li X, Dominguez DC, Ye B-C (2013) A PDMS/paper/glass hybrid microfluidic biochip integrated with aptamer-functionalized graphene oxide nano-biosensors for one-step multiplexed pathogen detection. Lab Chip 13(19):3921–3928. doi:10.1039/c3lc50654a